

Interpretation of Raman spectra of disordered and amorphous carbon

A. C. Ferrari* and J. Robertson

Department of Engineering, University of Cambridge, Cambridge CB2 1PZ, United Kingdom

(Received 24 November 1999)

The model and theoretical understanding of the Raman spectra in disordered and amorphous carbon are given. The nature of the G and D vibration modes in graphite is analyzed in terms of the resonant excitation of π states and the long-range polarizability of π bonding. Visible Raman data on disordered, amorphous, and diamondlike carbon are classified in a three-stage model to show the factors that control the position, intensity, and widths of the G and D peaks. It is shown that the visible Raman spectra depend formally on the configuration of the sp^2 sites in sp^2 -bonded clusters. In cases where the sp^2 clustering is controlled by the sp^3 fraction, such as in as-deposited tetrahedral amorphous carbon (ta -C) or hydrogenated amorphous carbon (a -C:H) films, the visible Raman parameters can be used to derive the sp^3 fraction.

I. INTRODUCTION

The great versatility of carbon materials arises from the strong dependence of their physical properties on the ratio of sp^2 (graphitelike) to sp^3 (diamondlike) bonds.¹ There are many forms of sp^2 -bonded carbons with various degrees of graphitic ordering, ranging from microcrystalline graphite to glassy carbon. In general, an amorphous carbon can have any mixture of sp^3 , sp^2 , and even sp^1 sites, with the possible presence of up to 60 at. % hydrogen. The compositions are conveniently shown on the ternary phase diagram, Fig. 1. We define diamondlike carbon (DLC) as amorphous carbon with a significant fraction of sp^3 bonds. The hydrogenated amorphous carbons (a -C:H) have a rather small C-C sp^3 content. DLC's with higher sp^3 content are termed tetrahedral amorphous carbon (ta -C) and its hydrogenated analog ta -C:H. Another crucial parameter is the degree of clustering of the sp^2 phase, which should be added as a fourth dimension in the ternary phase diagram.¹ Amorphous carbons with the same sp^3 and H content show different optical, electronic, and mechanical properties according to the clustering of the sp^2 phase.

Raman spectroscopy is a standard nondestructive tool for the characterization of crystalline, nanocrystalline, and amorphous carbons.²⁻¹⁴ The Raman spectrum of diamond consists of the T_{2g} 1332-cm⁻¹ zone center mode.² The Raman spectra of disordered graphite show two quite sharp modes, the G peak around 1580–1600 cm⁻¹ and the D peak around 1350 cm⁻¹, usually assigned to zone center phonons of E_{2g} symmetry and K -point phonons of A_{1g} symmetry, respectively.³⁻⁶ The unusual fact is that G and D peaks, of varying intensity, position, and width, continue to dominate the Raman spectra of nanocrystalline and amorphous carbons, even those without widespread graphitic ordering.

The key property of interest in DLC is the sp^3 content.¹ This is usually measured by nuclear magnetic resonance (NMR) or electron-energy-loss spectroscopy (EELS), but these are time-consuming and destructive methods. Raman scattering is sometimes used to probe the sp^2/sp^3 fraction in DLC's. However, visible Raman spectroscopy is 50–230 times^{7,8} more sensitive to sp^2 sites, as visible photons preferentially excite their π states. uv Raman spectroscopy, with

its higher photon energy of 5.1 eV, excites both the π and the σ states and so is able to probe both the sp^2 and sp^3 sites, allowing a direct probe of the sp^3 bonding.^{15,16} Nevertheless, visible Raman spectroscopy is widely used on DLC's, and it would be very useful to have a framework in which at least indirectly derive the sp^3 fraction of DLC's.

The aim of this paper is to describe in detail the Raman process in disordered carbons. It is shown that the visible Raman spectrum depends fundamentally on the ordering of sp^2 sites and only indirectly on the fraction of sp^3 sites. We give a restricted range of conditions under which it is possible to use visible Raman spectroscopy to derive the sp^3 content. To do this, we first describe the atomic and electronic structure of amorphous carbon and then the nature of Raman scattering in disordered carbons, both of which show unique features. We then present a three-stage model relating the visible Raman parameters to the sp^2 nanostructure and content of disordered carbons. This is sufficiently general to hold for all amorphous carbons, both hydrogenated and hydrogen-free. This paper focuses on the G and D peaks, neglecting other features that are sometimes present, such as

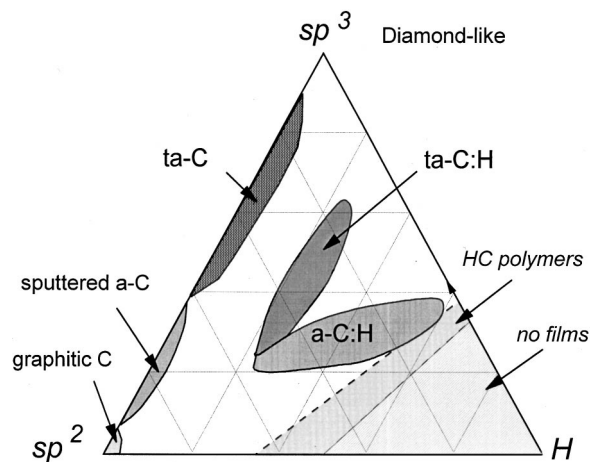


FIG. 1. Ternary phase diagram of amorphous carbons. The three corners correspond to diamond, graphite, and hydrocarbons, respectively.

those at 1100–1200 and 1400–1500 cm^{-1} , which will be discussed elsewhere.

II. ATOMIC AND ELECTRONIC STRUCTURE OF DISORDERED CARBONS

Disordered carbons have sp^3 and sp^2 sites. The sp^3 sites have only σ states while the sp^2 sites also possess π states. It is often possible to treat σ and π states separately. σ and π bonds have a significantly different behavior. σ bonds are two-center bond orbitals between adjacent atoms. In the bond-orbital approximation,^{17,18} any property of occupied states such as the total energy, charge density, or polarizability can then be expressed as simply the sum of independent, short-range terms for each bond. There are no long-range forces in this approximation, and the electron structure depends only on short-range order.

π states are different, because a π orbital usually interacts with π states on more than one atom to form a conjugated system such as benzene. Then, one can no longer define unique bond orbitals. Conjugated bonds cannot now be expressed as the sum of independent, two-center bonds. Each bond contains contributions from adjacent bonds, and this gives rise to longer-range forces and long-range polarizabilities.¹⁹

The medium-range order due to π -bonding distinguishes disordered carbons from the σ -bonded disordered semiconductors like a -Si. π bonding is maximized if the π states form pairs of aligned π states, or sixfold aromatic rings or graphitic clusters of aromatic rings.¹⁷ This occurs in microcrystalline graphite and in annealed DLC's. However, as-deposited DLC's are more disordered than this "cluster model."²⁰

Figure 2(b) shows the band structure of a single graphite layer.¹⁷ The σ and π states act separately. The σ states lie well away from the Fermi level and have gap of 6 eV. π states and empty π^* states form bands that touch at the Brillouin zone K . The π band energies along ΓKM in nearest-neighbor tight-binding approximation are

$$E = \pm \gamma |1 + 2 \cos(ka)|, \quad (1)$$

where γ is the $pp\pi$ interaction, a is the lattice spacing, and k is the wave vector. In graphitic clusters, the π states have minimum band energies of roughly¹⁷

$$E_g \approx \frac{2\gamma}{M^{1/2}} \approx 2\gamma \left(\frac{a}{L_a} \right), \quad (2)$$

where M is the number of aromatic rings in the cluster and L_a is the cluster diameter or in-plane correlation length.

We consider aromatic clusters as parts of a graphite superlattice. Hence, from Eqs. (1) and (2), the energy states of the clusters can be mapped onto those of graphite by

$$1 + 2 \cos(ka) = - \frac{a}{L_a} \quad (3)$$

or $\sin(\Delta ka) \approx a/(\sqrt{3}L_a)$ for small Δk , where Δk is the k distance away from K , and $K = (\frac{2}{3}, \frac{2}{3})\pi/a$. Smaller clusters correspond to k 's further away from K .

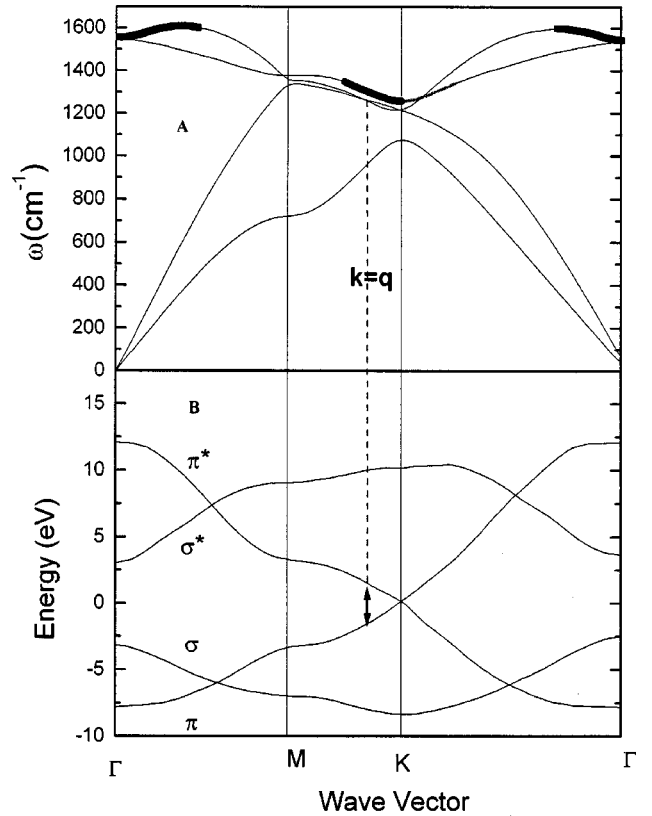


FIG. 2. (a) Phonon dispersion (Ref. 21) and (b) electronic band structure (Ref. 17) of a single graphite layer. Similar phonon dispersion of graphite is found in the *ab initio* calculations of Kresse, Furthmüller, and Hafner (Ref. 22). The bold lines from Γ and K mark the mapping of the E_{2g} and A_{1g} -like eigenvectors of aromatic clusters on those of graphite, according to Mapelli *et al.* (Ref. 21). The bold line from K to M corresponds to phonons selected by the $k=q$ "quasi selection rule," as shown by the dashed vertical line. The phonons on the right of K , from K to Γ , are also selected by the $k=q$ "quasi selection rule," but do not correspond to modes with high modulation of polarizability.

The long-range effects in conjugated systems can be formalized by defining a mobile bond order P_{uv} between two orbitals¹⁹ u, v :

$$P_{uv} = 2 \sum_{\text{occ}} c_u c_v \quad (4)$$

and a bond-bond polarizability $\Pi_{uv,wx}$ between bonds uv and wx :

$$\Pi_{uv,wx} = \frac{\partial^2 E}{\partial \gamma_{uv} \partial \gamma_{wx}}, \quad (5)$$

for wave functions $\psi = \sum c_u \phi_u$, where the sums are over occupied states.¹⁹ E is the sum of energies of occupied states and γ_{uv} is the nearest-neighbor interaction along bond uv . The difference between σ and π states is that for σ states $P_{uv} \approx 0$ if orbitals u and v are on different bonds, while in conjugated π systems, $P_{uv} \neq 0$, and it decreases gradually with the separation of u and v .

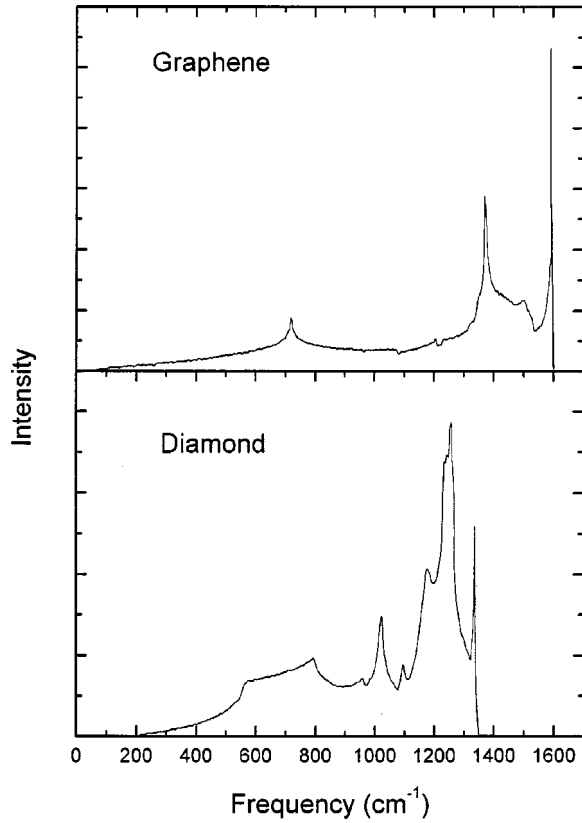


FIG. 3. Phonon density of states of a single graphite layer (graphene) (Ref. 21) and of diamond (Ref. 23).

III. VIBRATIONAL MODES

Figure 3 shows the vibrational density of states (VDOS) of graphite and diamond.^{21–23} The VDOS of diamond extends beyond its Raman frequency, 1332 cm^{-1} , to $\sim 1360 \text{ cm}^{-1}$. Figure 2(a) also shows the phonon dispersion curves of a graphite layer.²¹ The graphite VDOS extends beyond its Γ -point Raman frequency up to a band limit of $\sim 1620 \text{ cm}^{-1}$, due to the upwards phonon dispersion away from Γ . Graphite has a higher VDOS band limit than diamond because the sp^2 sites have stronger, slightly shorter bonds than sp^3 sites.

The DOS of alloys can be of two types. If the coupling between sites is small, the alloys are in the atomic limit, so the alloy DOS resembles a compositionally weighted mixture of the DOS of each component. If the coupling is strong, then the alloy DOS and the band limits interpolate smoothly between the two components. The Raman spectra suggest that the VDOS of DLC's are in the atomic limit, in that specific features, such as the G mode of sp^2 sites, remain at all sp^2 contents. Thus, the band limit does not change linearly with sp^3 content from 1600 to 1360 cm^{-1} . This is partly because sp^2 sites tend to cluster in a sp^3 matrix in DLC's.¹⁷ A consequence is that the vibrations of sp^2 sites remain around 1600 cm^{-1} and lie above the band limit of the sp^3 matrix. This causes these modes to be localized on the sp^2 sites and above the extended modes of the sp^3 matrix.²⁴ The band limit thus cannot be used as a way to get the sp^3 fraction, as sometimes suggested.²⁵ We therefore need a different approach in which the changes in the visible Raman spectra are related primarily to the changes of the sp^2 phase and only weakly to the sp^3 phase.

The vibrational modes of covalent solids are often modeled as a valence force field of bond-stretching and bond-bending forces. These forces are usually short-ranged for σ -bonded systems.²⁶ On the other hand, a valence force field for graphite typically uses forces up to fifth-nearest neighbors.^{27,28} Recently Mapelli *et al.*²¹ were able for the first time to provide a common force field for aromatic molecules and graphite by using forces proportional to the bond orders P_{uv} and bond-bond polarizabilities $\Pi_{uv,wx}$, Eqs. (4) and (5). As Π is directly related to the electronic structure and tight-binding parameter γ , this method provides a formal relationship between longer-range forces, so they are not just adjustable parameters.

IV. RAMAN SCATTERING IN DISORDERED CARBON

Raman modes in single crystals obey the fundamental selection rule $\mathbf{q} \approx \mathbf{0}$, where q is the wave vector of the scattered phonon. In a finite-size domain, the selection rule is relaxed to allow the participation of phonons near Γ , with $\Delta q \approx 2\pi/d$, where d is the dimension of the crystalline domain. Nemanich, Solin, and Martin²⁹ (NSM) showed that the Raman scattering intensity of a finite crystal is given by

$$I(\omega) = \frac{n(\omega) + 1}{\omega} \sum_{\mathbf{q}, j} C(\mathbf{q}, \omega_j(\mathbf{q})) |F(\mathbf{q})|^2 \times \frac{\Gamma/2\pi}{[\omega - \omega_j(\mathbf{q})]^2 + \Gamma^2/4}, \quad (6)$$

where $C(\mathbf{q}, \omega_j(\mathbf{q}))$ is the Raman coupling coefficient for a phonon of wave vector \mathbf{q} and branch j , and $|F(\mathbf{q})|^2$ is the wave-vector uncertainty of the phonons involved in the light scattering. $n(\omega) + 1$ is the boson occupation factor, and Γ is the phonon lifetime broadening. In amorphous materials, the wave-vector uncertainty is $\Delta q \approx 1/a$, where a is the bond length, and now all phonon modes can participate in the Raman spectrum. The intensity is now given by the matrix-element-weighted vibrational density of states according to the Shuker-Gammon formula³⁰

$$I(\omega) = \frac{n(\omega) + 1}{\omega} C(\omega) G(\omega). \quad (7)$$

Here, $G(\omega)$ is the VDOS of the disordered network. Equation (7) describes quite well the Raman spectra of a -Si and a -Ge, which are sp^3 bonded only, by using a broadened version of the crystalline VDOS as $G(\omega)$.²⁶

The visible Raman spectra of disordered carbons are in marked contrast. The VDOS of disordered carbon with various sp^3 contents consists of smooth, broad features.^{31,32} In contrast, the Raman spectra of all disordered carbons are dominated by the relatively sharp G and D features of the sp^2 sites. This could be ascribed to the much greater cross section of the π states.^{7,8} Nevertheless, the prevalence of G - and D -like features, even in amorphous carbons with little graphitic ordering, requires explanation.

The G mode of graphite at 1581 cm^{-1} has E_{2g} symmetry. Its eigenvector shown in Fig. 4(a) involves the in-plane bond-stretching motion of pairs of C sp^2 atoms. This mode does not require the presence of sixfold rings, and so it oc-

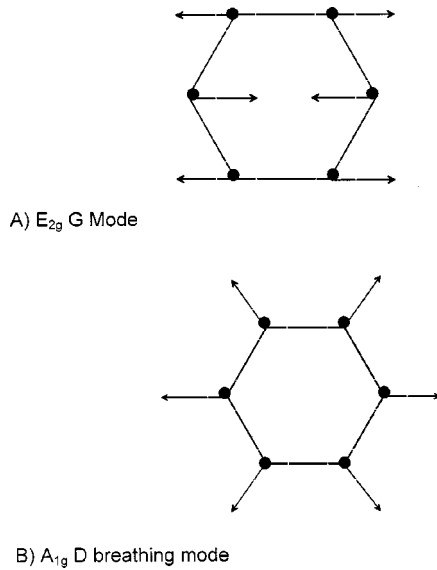


FIG. 4. Carbon motions in the (a) G and (b) D modes. Note that the G mode is just due to the relative motion of sp^2 carbon atoms and can be found in chains as well.

occurs at all sp^2 sites, not only those in rings. It always lies in the range $1500\text{--}1630\text{ cm}^{-1}$, as it does in aromatic and olefinic molecules.³³

The D peak around 1355 cm^{-1} is a breathing mode of A_{1g} symmetry involving phonons near the K zone boundary, Fig. 4(b). This mode is forbidden in perfect graphite and only becomes active in the presence of disorder. The D mode is dispersive; it varies with photon excitation energy, even when the G peak is not dispersive.^{34–37} We will see that its intensity is strictly connected to the presence of sixfold aromatic rings. Tuinstra and Koenig³ (TK) noted that the ratio of its intensity to that of the G peak varied inversely with L_a :

$$\frac{I(D)}{I(G)} = \frac{C(\lambda)}{L_a}, \quad (8)$$

where $C(515.5\text{ nm}) \sim 44\text{ \AA}$.^{2,3,37} The D peak was first attributed to a A_{1g} breathing mode at K , activated by the relaxation of the $q=0$ selection rule.³ It was then linked to maxima in the VDOS of graphite at M and K points.^{4,27} However, this does not account for the dispersion of the D position with photon energy, why the D peak overtone, seen even where no D peak is present, is dispersive, or why the $I(D)/I(G)$ ratio (8) is dispersive.³⁴ Phonon confinement (6) does not explain why the D mode is more intense than others with smaller Δq . It also does not explain why the D mode is seen in disordered graphite with $L_a \approx 30\text{ nm}$,⁶ when the NSM formula (6) would limit the participating phonons to a much narrower Δq range around Γ .

Figure 2(a) shows the phonon dispersion of a single layer of graphite. Baranov *et al.*,³⁵ Pocsik *et al.*,³⁶ and Matthews *et al.*³⁷ proposed that the D peak arises as resonant Raman coupling by a strong enhancement of the Raman cross section of the phonon of wave vector q , when it equals the wave vector k of the electronic transition excited by the incident photon ($k=q$ “selection rule”).

We now give a more detailed account. In particular, we propose a physical mechanism to explain the $k=q$ “quasi selection rule;” we identify a different branch in the dispersion relation as the origin of D peak (in contrast to Refs. 36 and 37). We formally show which real-space motions give rise to the D peak, and we propose, on the basis of the “quasi selection rule,” an interpretation to some experimental findings.

Raman scattering is the inelastic scattering of photons by phonons due to the change of polarization caused by the phonon mode.³⁸ When the photon energy is above the band gap, electrons of all wave vectors can be excited. However, in graphite, the band gap lies in the visible range only within a small part of k space around the K point, Fig. 2(b). All these bands have π character. In this case, photons resonantly excite states only at the k vector where the band gap equals the photon energy. This sets up a polarization density wave of this k vector. Its intensity is strong because of the long-range polarizability of π states.

The change of bond polarization with bond length is by far the dominant term in the Raman matrix element for π states.²⁶ This term is large for the breathing mode of sixfold rings. By symmetry, for a breathing mode of a graphite plane, the contributions from each ring add constructively because of the long-range polarization. On the other hand, by symmetry, contributions from rings of other orders within a graphite plane tend to cancel. Thus, the polarization wave and Raman coupling have long-range coherence for breathing modes due to the π bonding and the symmetry of the graphite sheet. The greatest coupling is when the electron and phonon states are in phase over the range of polarization. This leads to the “quasi selection rule,” $k=q$, for the breathing modes of graphene sheets, Fig. 2. For first-order scattering, the fundamental selection rule must be relaxed to allow non- $(q=0)$ phonons to contribute. This means that we also need disorder to allow the enhancement of $k=q$ phonons.

Turning to graphitic clusters, we noted above that the electronic states of graphitic clusters of size L_a can be mapped onto the modes of graphite at wave vector k by Eq. (3). Mapelli *et al.*²¹ showed that the eigenvectors of the main Raman modes of aromatic oligomers have the same symmetry as the E_{2g} and A_{1g} Raman modes of graphite. They also showed that the eigenvectors of these oligomers or clusters can be mapped onto those of graphite phonons along the direction ΓKM . In particular, the A_{1g} -type breathing modes of the aromatic clusters map onto phonons between K and $(K-M)/2$, and the E_{2g} -type modes map onto phonons from Γ to $(\Gamma-K)/4$ (branches shown in bold in Fig. 2). Our relationship (3) can be used to map the A_{1g} -like modes, thus providing a way to visualize the real-space motion along that branch. This indicates that aromatic clusters can be considered as a part of a graphite superlattice, both electronically and vibrationally. This simultaneous mapping means that the behavior and dispersion of the D and G peaks in graphite also holds for aromatic oligomers and clusters in disordered carbon.

Band and phonon dispersions are rather isotropic around K . As the photon energy rises, the $k=q$ selection rule selects a ring of phonons around the K point. The symmetric breathing modes have the highest modulation of the polarizability and therefore have the highest Raman cross section. This suggests that modes between K and M give the highest con-

tribution to the D peak and possibly explains why the intensity of D peak is higher than modes from other branches of the dispersion curves but with the same q . Note that previous works^{36,37} assigned the D peak to all the modes around K in the lower optical branch, which touches the acoustic branch at K . To select the correct optical branch we cannot just rely on the coincidence between its calculated dispersion and the experimental positions of D peak. The A_{1g} mode is singly degenerate. We thus need a band *singly degenerate* at K and *upwards dispersing* away from K . The branch chosen by Refs. 36 and 37 leads to a doubly degenerate E mode at K .²¹ The upper branch in Ref. 37 disperses downwards, but the *ab initio* calculations of Mapelli *et al.*²¹ and Kresse, Furthmüller, and Hafner²² reproduce the symmetry and upwards dispersion, Fig. 2.

Applying the $k=q$ selection rule to all the phonon branches of graphite, we can account for other features of the Raman spectrum. First, considering the $\sim 2400\text{-cm}^{-1}$ peak as an overtone of the lower acoustic branch away from K , we can explain its redshift³⁹ with increasing laser energy due to the opposite dispersion of this phonon branch. Second, a Stokes shift with lower frequency than the anti-Stokes shift was reported for the D peak, and vice versa for the 2400-cm^{-1} peak.³⁹ We can now explain the slight difference in the Stokes and anti-Stokes energies due to the slope of the phonon and electron dispersion relations away from K . Finally, in graphite or disordered graphite with a high c -axis ordering, the D peak and its second-order peak are doublets.^{6,34,39} This was originally attributed to two maxima in the VDOS at K and M .²⁷ However, we attribute these doublets to the splitting of phonon and electron branches of given wave vector by interlayer interactions when three-dimensional stacking occurs.^{21,35} This causes doublets to act as signatures of c -axis ordering.⁶

So far we implicitly assumed graphite to be the reference to explain the Raman features in micro/nanocrystalline graphite. The main consequence is that the D peak arises from aromatic rings. Starting from graphite, at a fixed λ , $I(D)/I(G)$ will increase with increasing disorder, according to TK Eq. (8). For more disorder, clusters decrease in number become smaller and more distorted, until they open up. As the G peak is just related to the relative motion of $C sp^2$ atoms, the $I(D)$ will now decrease with respect to $I(G)$ and the TK relationship will no longer hold, as shown in Fig. 5. For small L_a , the D -mode strength is proportional to the probability of finding a sixfold ring in the cluster, that is, proportional to the cluster area. Thus, in amorphous carbons the development of a D peak indicates ordering, exactly opposite from the case of graphite.

We can finally summarize the main factors modifying $C(\omega)$:

- (1) sp^2 sites are resonantly enhanced over sp^3 ones,
- (2) within the sp^2 matrix, $q=k$ modes are enhanced over the others, and
- (3) breathing modes are enhanced within $q=k$ modes.

V. SPECTRUM FITTING

A practical point when comparing different fitting parameters for Raman spectra is to know the fitting procedures used. The Raman spectrum is a VDOS modified by a cou-

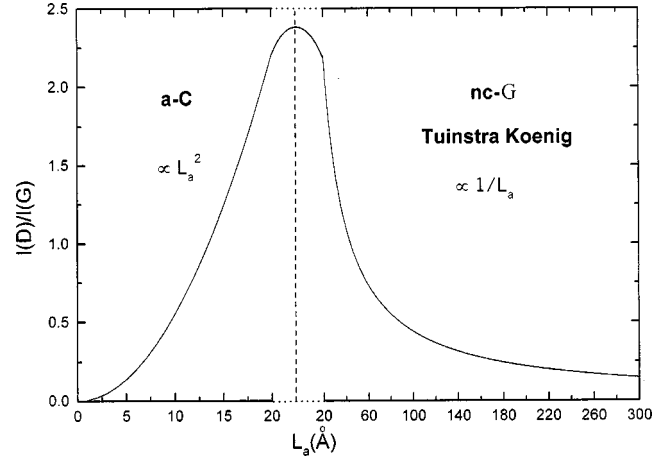


FIG. 5. Variation of the $I(D)/I(G)$ ratio with L_a . The broad transition between the two regimes is indicated.

pling coefficient, which incorporates various resonances. There is no *a priori* reason to choose a particular function to fit the spectrum. Empirically, the visible Raman spectra of amorphous carbons show one or two prominent features (the G and D peaks) and some minor modulations (usually around $1100\text{--}1200$ and $1400\text{--}1500\text{ cm}^{-1}$). The simplest fit consists of two Lorentzians or two Gaussians. A Lorentzian fit is often used for crystals, arising from finite lifetime broadening, and it is normally used for disordered graphite. A Gaussian line shape is expected for a random distribution of phonon lifetimes in disordered materials. A simple two-symmetric-line fit is not always suitable, and one can find a multipic fit (typically four: $D, G+2$ at ~ 1100 and $\sim 1400\text{ cm}^{-1}$).

The most widely used alternative to a Gaussian fit is a Breit-Wigner-Fano (BWF) line for the G peak and a Lorentzian for the D peak.^{40–42} The BWF line has an asymmetric line shape, which should arise from the coupling of a discrete mode to a continuum.⁴³ The BWF line shape is given by

$$I(\omega) = \frac{I_0 [1 + 2(\omega - \omega_0)/Q\Gamma]^2}{1 + [2(\omega - \omega_0)/\Gamma]^2}, \quad (9)$$

where I_0 is the peak intensity, ω_0 is the peak position, Γ is assumed as the full width at half maximum (FWHM) and Q^{-1} is the BWF coupling coefficient. The Lorentzian line shape is recovered in the limit $Q^{-1} \rightarrow 0$. We emphasize that several points should be considered with Eq. (9). First, the BWF curve tails increasingly to lower frequencies for lower Q values. This allows a BWF line to account for residual Raman intensity at ~ 1100 and 1400 cm^{-1} , without two extra peaks. The BWF+Lorentzian line pair is therefore an excellent means to fit Raman spectra of all carbons, from graphite to *ta*-C. A Lorentzian line shape is used for the D peak as it is from the same family as the BWF line, while the various enhancement mechanisms for the D peak are consistent with a Lorentzian. However, any wide low-frequency tail of the BWF line will push the D peak to lower frequencies as the disorder increases. This significantly decreases the D peak size compared to a two-Gaussian fit. In general, the D -peak position will decrease with increasing disorder with the BWF+Lorentzian fit, but will increase (up to 1400 cm^{-1} or more) for the double-Gaussian fit.^{9,10,13} Note that the fit of the D peak and especially its position is the least accurate for

many amorphous carbons, because it is often only a low-frequency shoulder of the G peak. Two factors can shift the D peak. On one hand, smaller aromatic clusters have higher modes²¹ and shift D upwards. On the other hand, a decrease in number of ordered aromatic rings on passing from nanocrystalline graphite to a -C lowers D and reduces its intensity, due to softening of the VDOS.⁴⁴

Another important issue from Eq. (9) is that the maximum of the BWF line is not at ω_0 but lies at lower frequencies:

$$\omega_{\max} = \omega_0 + \frac{\Gamma}{2Q}, \quad (10)$$

as Q is negative. We define the G position as ω_{\max} rather than ω_0 . ω_0 is higher than the apparent peak maximum because ω_0 is the position of the undamped mode.⁴³ We attribute no physical meaning to the undamped frequency but merely view the BWF line as an efficient way to fit the data. The asymmetric BWF line shape is appropriate for the G peak due to the asymmetry of the VDOS of graphite or amorphous carbons towards lower wave numbers.⁹ No Fano resonance is present. Whenever reporting data from other papers using BWF fits, we will use ω_{\max} , derived by applying Eq. (10) to their data. Moreover, ω_{\max} compares directly with data from symmetric curve fitting.

Finally, it is not always clear if the $I(D)/I(G)$ ratio should be the ratio of the peak heights or peak areas. Generally, groups using BWF+Lorentzian fits report peak height ratios, while groups using two Gaussians report the area ratio. The difference is not so important for disordered graphite, as the peak widths are similar, but this is not so for amorphous carbons. In that case, the broadening of the D peak is correlated to a distribution of clusters with different orders and dimensions, and thus the information about the less distorted aromatic rings is in the intensity maximum and not in the width, which depends on the disorder. Ring orders other than six tend to decrease the peak height and increase its width. Unless differently stated, in this paper we refer to $I(D)/I(G)$ as the ratio of peak heights.

VI. THREE-STAGE MODEL

The large amount of experimental visible Raman spectra on amorphous carbons will be interpreted using a phenomenological three-stage model. Given a perfect, infinite graphite sheet, we consider the introduction of a series of defects: bond-angle disorder, bond-length disorder, and hybridization. We neglect the possible role of hydrogen, as C-H modes give no detectable contributions in the G and D peaks (Sec. VIII). The Raman spectrum is considered to depend on

- (1) clustering of the sp^2 phase,
- (2) bond disorder,
- (3) presence of sp^2 rings or chains, and
- (4) the sp^2/sp^3 ratio.

These factors act as competing forces on the shape of the Raman spectra, as shown schematically in Fig. 6. We define an *amorphization trajectory*⁶ ranging from graphite to ta -C (or diamond) consisting of three stages, as shown in Fig. 7:

- (1) graphite \rightarrow nanocrystalline graphite (nc - G),
- (2) nanocrystalline graphite \rightarrow a -C, and

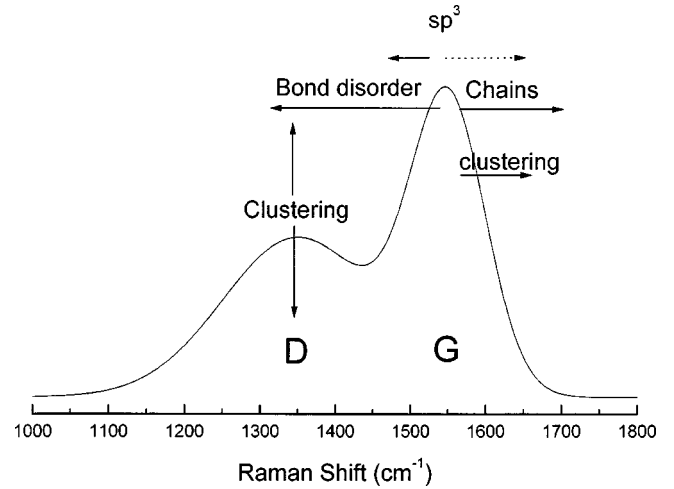


FIG. 6. Schematic diagram of influences on the Raman spectra. A dotted arrow marks the indirect influence of the sp^3 content on increasing G position.

- (3) a -C \rightarrow ta -C (\rightarrow $\sim 100\%$ sp^3 ta -C, defected diamond⁴⁵).

For simplicity, we will consider the evolution of G -peak position and $I(D)/I(G)$. Except where differently stated, we refer to Raman data at 514 nm.

A. Stage 1: From graphite to nanocrystalline graphite

The main effects in the evolution of the Raman spectrum in this stage are the following.

- (a) The G peak moves from 1581 to ~ 1600 cm^{-1} .
- (b) The D peak appears and $I(D)/I(G)$ increases following the TK equation (8).
- (c) There is no dispersion of the G mode.

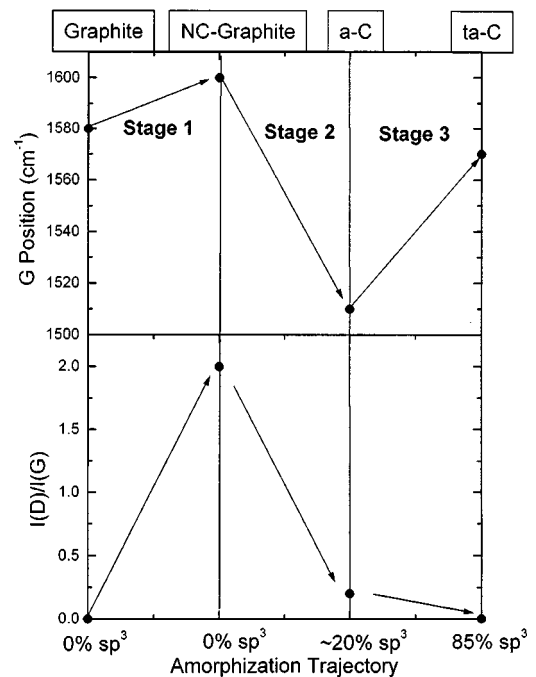


FIG. 7. Amorphization trajectory, showing a schematic variation of the G position and $I(D)/I(G)$ ratio.

These effects, at a fixed wavelength, can be explained by the VDOS of graphite and phonon confinement.^{5,6} First, the shift of G is really the appearance of a second peak, D' , at $\sim 1620 \text{ cm}^{-1}$, which merges in the G peak for small grains. A single line fit to $G+D'$ feature gives a net increase of G position. The appearance of D' occurs because the relaxation of the $q=0$ selection rule allows higher-frequency phonons, as phonons disperse upwards away from Γ ; see Figs. 2 and 3. The main structural change is passing from a monocrystalline to a polycrystalline material; there are virtually no sp^3 sites. The loss of three-dimensional ordering is indicated by the disappearance of the doublet in the D peak and in its second-order peak.⁶ There are many experimental results showing stage 1, such as those from Lespade and co-workers.^{5,6}

We note that there are only few experimental verifications of the TK equation (8), where L_a is known independently by x-ray diffraction (XRD),² and the minimum L_a for which the TK equation has been directly verified is $\sim 20 \text{ \AA}$. TK assumes that graphite becomes uniformly nanocrystalline. However, for a system with mixed grain sizes, with volume fractions X_i and dimensions L_{ai} , the effective L_a is given by

$$\frac{1}{L_{a,\text{eff}}} = \sum_i^N X_i \frac{1}{L_{ai}}. \quad (11)$$

We can thus explain why, since XRD weights more the bigger crystallites, the TK equation will underestimate L_a due to the dominant effect of small crystallites.⁴⁶

B. Stage 2: From nanocrystalline graphite to a -C

In this stage, defects are progressively introduced into the graphite layer, causing its phonon modes to soften, particularly the G peak. The Shuker-Gammon formula (7) applies, and the VDOS is no longer that of graphite. The end of stage 2 corresponds to a completely disordered, almost fully sp^2 -bonded a -C consisting of distorted sixfold rings or rings of other orders (maximum 20% sp^3). A typical example is sputtered a -C.⁴⁷ The main effects in the evolution of the Raman spectrum are

- (a) The G peak decreases from 1600 to $\sim 1510 \text{ cm}^{-1}$.
- (b) The TK equation is no longer valid: $I(D)/I(G) \propto M \propto L_a^2$.
- (c) $I(D)/I(G) \rightarrow 0$.
- (d) Increasing dispersion of the G peak occurs.

Another effect is the absence of well-defined second-order Raman peaks, but a small modulated bump from ~ 2400 to $\sim 3100 \text{ cm}^{-1}$.

Increasing bond-angle and bond-bending disorder and the presence of nonsixfold rings softens the VDOS.^{44,24} The introduction of sp^3 sites into a structure composed only of sixfold rings further softens the VDOS.^{24,44}

Increasing the defects and reducing L_a below 2 nm, the number of ordered rings now decreases and $I(D)$ starts to decrease. The G peak relates only to bond stretching of sp^2 pairs, so G retains its intensity, and $I(D)/I(G)$ decreases with increasing amorphization (Fig. 5). The TK equation is no longer valid. This is the usual situation with a -C. Development of the D peak indicates disordering of graphite but

ordering of a -C. This is expressed in effect (b) by the proportionality of $I(D)/I(G)$ to M , the number of ordered rings. In fact, $I(D)/I(G)$ is proportional to the number and clustering of rings, but the main disordering effect in stage 2 can be taken as the decrease of number of ordered rings, since the dimensions are under 20 \AA . We propose a new relation for stage 2:

$$\frac{I(D)}{I(G)} = C'(\lambda) L_a^2. \quad (12)$$

Imposing continuity between Eqs. (8) and (12), we find $C'(514 \text{ nm}) \approx 0.0055$. At low excitation energy, the D peak is due to large aromatic clusters. Thus, combining Eqs. (2) and (12), $I(D)/I(G)$ will vary with the optical gap as

$$\frac{I(D)}{I(G)} = \frac{C''}{E_g^2}. \quad (13)$$

We have verified Eq. (13) by studying the clustering of sp^2 sites in ta -C deposited at elevated temperatures.⁴⁸ It is clear that this is an ideal situation in which thermal energy favors the clustering of the sp^2 phase into ordered rings, and so Eq. (13) holds. This is not so in general, especially for as-deposited samples, where the ion-induced disorder in the sp^2 phase invalidates the simple relation (2) between cluster size and band gap.²⁰ In fact, as we will discuss in Sec. VI C, in going from as-deposited a -C's to ta -C we have always $I(D)/I(G) \sim 0$, but the gap increases. However, we stress that for visible Raman spectroscopy, whenever a D peak is present [$I(D)/I(G) \geq 0.1-0.2$], a decrease of the gap will always be reflected in an increase of $I(D)/I(G)$, even if not exactly in the form of Eq. (13). We will discuss elsewhere the progressive insensitivity of $I(D)/I(G)$ to the gap with increasing excitation energy.

Clear experimental examples of stage 2 are the ion implantation of glassy carbon^{40,41} (g -C) and sputtered a -C.^{49,31} Figure 8 plots data of McCulloch and co-workers^{40,41} on ion implantation of g -C at room temperature as a function of ion dose [Fig. 8(a)] and at a fixed dose with increasing implantation temperature [Fig. 8(b)]. We show the first and second stages of amorphization. The sp^3 content was checked by EELS and it rose to 15% only at the very end of stage 2. An NMR determination of sp^3 content in sputtered a -C with the G peak at $\sim 1500 \text{ cm}^{-1}$ and $I(D)/I(G) \sim 0$ gave $sp^3 \sim 7\%$.^{47,31}

The structure of a -C at the end of stage 2 consists of mainly sp^2 sites in puckered ring-like configurations (consisting of five-, six-, seven-, and eightfold disordered rings), and few if any sp^3 sites.^{47,44,50,51} Li and Lannin⁴⁷ showed an absence of ordered, planar sixfold rings [consistent with $I(D)/I(G) \sim 0$] and few chainlike structures.

C. Stage 3: From a -C to ta -C

In passing from a -C to ta -C, the sp^3 content rises from $\sim 10-20\%$ to $\sim 85\%$, while the sp^2 sites change gradually from rings to chains. The π states become increasingly localized on olefinic sp^2 chains and, eventually, sp^2 dimers embedded in the sp^3 matrix.^{24,51-54,15} The sp^2 modes lie above the sp^3 modes and become localized.²⁴ Olefinic C=C bonds are shorter than aromatic bonds, so they have higher

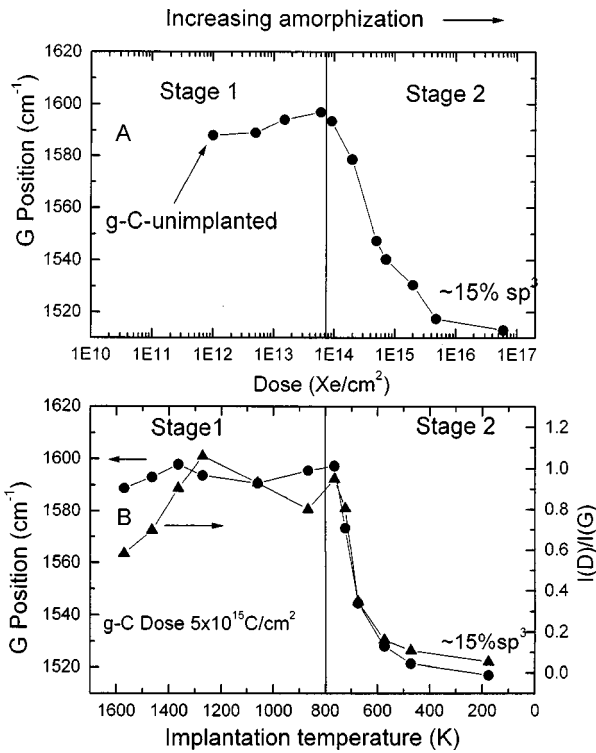


FIG. 8. Variation of the G position and $I(D)/I(G)$ ratio with (A) ion dose and (B) implant temperature for ion-bombarded glassy carbon, after McCulloch and co-workers (Refs. 40 and 41).

vibration frequencies.^{33,55} The main effects in the evolution of the Raman spectrum are as follows.

- The G peak increases from ~ 1510 to ~ 1570 cm^{-1} (or ~ 1630 cm^{-1} for sp^2 dimers in ion-implanted diamond.⁴⁵)
- $I(D)/I(G)$ is very low or 0.
- Dispersion of the G peak occurs.

The main change, i.e., the increase of the G -peak position with sp^3 content, is due to the change of sp^2 configuration from rings to olefinic groups, with their higher vibrational frequencies lying above the band limit of graphite. This effect is larger than the tendency of the G peak to fall due to mixing with lower-frequency sp^3 modes. This emphasizes the importance of the localization of sp^2 modes above the sp^3 modes, which minimizes the mixing of sp^2 with sp^3 modes. It follows that the model of Richter *et al.*²⁵ does not hold in practice.

The second major change is the absence of a D peak in a BWF fit. The G skewness falls to almost 0 at high sp^3 content.⁴² Also, the G -peak width first increases and then falls, as the G modes become localized on sp^2 dimers or shorter sp^2 chains with a sharper length distribution. A single-Gaussian fit is poor, although it still gives a fair representation of peak position and FWHM.⁵⁶

It has been argued that the high frequency of the G peak in ta -C is due to its high compressive macroscopic stress.^{56,14} We disagree with this, as it is found that the G peak does not move if the stress is removed by annealing.⁵⁷⁻⁵⁹ We verified that annealing up to complete stress release induces minimal structural changes in ta -C.⁵⁷ Also, the G peak of ta -C is blueshifted in both uv Raman spectra (~ 1660 cm^{-1} , compared to ~ 1590 cm^{-1} for sp^2 -bonded a -C) and 514-nm Ra-

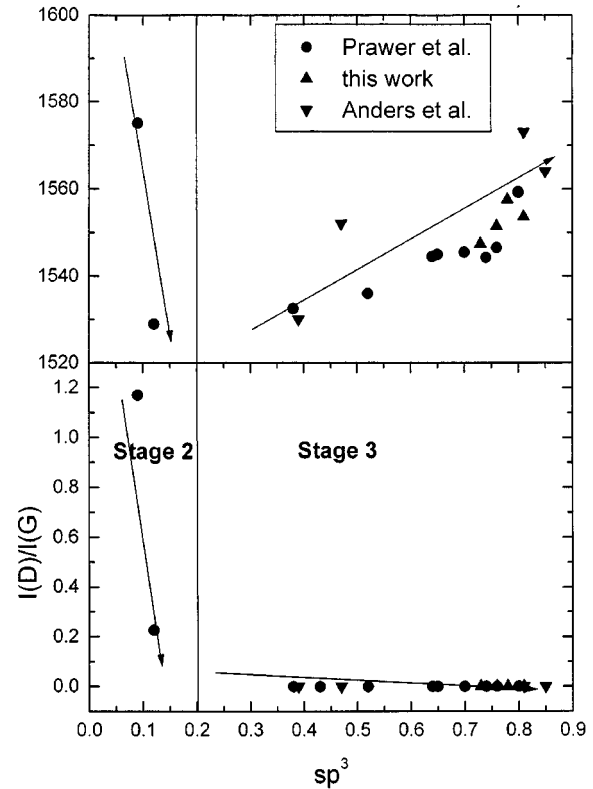


FIG. 9. Variation of the G position and $I(D)/I(G)$ ratio with sp^3 fraction for as-deposited a -C. Data from Prawer *et al.* (Ref. 42), this work, and Anders and co-workers (Refs. 56 and 59).

man spectra (~ 1570 cm^{-1} compared to ~ 1510 cm^{-1}). This dispersion can only be fully explained by contributions of olefinic sp^2 groups, whose higher vibration frequencies lie above the graphite band limit.¹⁵ Tallant *et al.*⁶⁰ suggested to fit the Raman spectra of as-deposited ta -C using the frequencies of embedded ideal five-, six-, and sevenfold sp^2 rings. Such a model, even if very good fits are obtained for the 514-nm Raman spectra, cannot explain the dispersion above ~ 1580 cm^{-1} seen in the uv Raman spectra and is thus incorrect for ta -C. uv Raman spectroscopy gives not only an evenly weighted probe of sp^3 and sp^2 sites, but also an evenly weighted probe of ring and chain sp^2 modes, not biased towards sp^2 configurations of lower band gap. It shows a G peak at 1660 cm^{-1} in ta -C, indicating a preponderance of chain groups.

Figure 9 shows our 514-nm Raman data on ta -C deposited by a filtered cathodic vacuum arc (FCVA), together with data of Prawer *et al.*⁴² and Anders and co-workers^{59,56} on (t) a -C deposited by FCVA. We only included data with sp^3 content known by EELS. Figure 9 is a clear example of the transition from stage 2 to stage 3 in accordance with the above trends. Note the absence of the D peak in ta -C's. Although $I(D)/I(G) \sim 0$, typically we have an increase in the gap from ~ 0.5 to ~ 2.5 eV, going from a -C to ta -C. This would contradict Eq. (13). However, this is expected since the gap is controlled by the π -electron delocalization, not necessarily in well-ordered rings, but on the whole sp^2 phase. An increasing sp^2 content, even if not via an ordered sp^2 matrix, causes a decrease of the gap reflected in a softening of the G mode and an increase in its FWHM.

Figure 7 summarized the behavior of G peak position and $I(D)/I(G)$ through all the three stages. It shows no unique

relationship between the G -peak position and sp^3 content. G -peak position can either increase or decrease with increasing sp^3 and a high and low sp^3 content corresponds to the same G position. $I(D)/I(G)$ would discriminate, between high and low content and, except for the first stage, in which sp^3 is constant anyway, it would be a crucial parameter to quantify the sp^3 phase. Figure 7 also emphasizes that most changes of the Raman spectra are not driven by the sp^3 increase, but by the evolution of sp^2 clusters.

Figure 7 shows how we could relate the $[G, I(D)/I(G)]$ pair to sp^3 content. However, the situation is more complex than described so far, as the clustering of the sp^2 phase has to be taken directly into account, as we discuss now.

VII. THE HYSTERESIS CYCLE

The amorphization trajectory discussed above is derived for disordering (e.g., ion implantation) in relatively ordered carbons or for room-temperature depositions. What happens if we follow an *ordering trajectory* from ta -C to graphite? Examples of an ordering trajectory are deposition at high temperature, annealing after deposition, low-dose ion implantation of ta -C, or unfiltered deposition processes. These cases favor clustering of sp^2 sites into fairly ordered aromatic rings.

There are two fundamental processes: (a) sp^3 sites convert to sp^2 sites and (b) sp^2 cluster size increases and the sp^2 phase eventually orders in rings. There are two situations. During a room-temperature deposition of ta -C, the sp^2 and sp^3 phases are linked together, forcing the sp^2 phase to evolve continuously with increasing sp^3 content, giving the trends seen in Fig. 7. On the other hand, other treatments, such as annealing or high-temperature deposition, separate the two processes so that clustering (b) occurs at lower temperatures than conversion (a).^{48,57} This causes *hysteresis*. Visible Raman spectroscopy is much more sensitive to clustering than conversion. The effect of the hysteresis is that there is no unique relation between $I(D)/I(G)$ or the G position and sp^3 fraction (Fig. 10). Thus, we need an independent assessment of the sp^3 fraction. Fundamentally, optical and electrical properties correlate closely with the degree of sp^2 clustering, and not directly with the sp^3 content. This implies that *in general visible Raman spectroscopy is not a safe way to get sp^3 content*. Various examples of hysteresis can be found in the literature;^{14,48,57,61,62} see Fig. 11.

We have so far neglected the presence of sp^1 bonds, whose C-C vibrations at 2100–2200 cm^{-1} (Ref. 33) lie outside the G and D regions. Even if present in a small amount, this does not change our model.

Generally, in an inhomogeneous material we predict the TK equation to underestimate L_a with respect to XRD, as for Eq. (11). This gives a hysteresis even in stage 1, in that visible Raman spectroscopy is more sensitive to the smaller graphitic domains in a material not composed of grains having a similar L_a .

Are there conditions for estimating sp^3 content by visible Raman spectroscopy? Figures 7 and 9 show that a high G -peak position combined with a $I(D)/I(G) \sim 0$ is a sufficient condition to assess the sp^3 content of ta -C. In this case, the sp^3 content can be read off from Fig. 9(a). Here, a higher G position correlates with a higher optical gap.

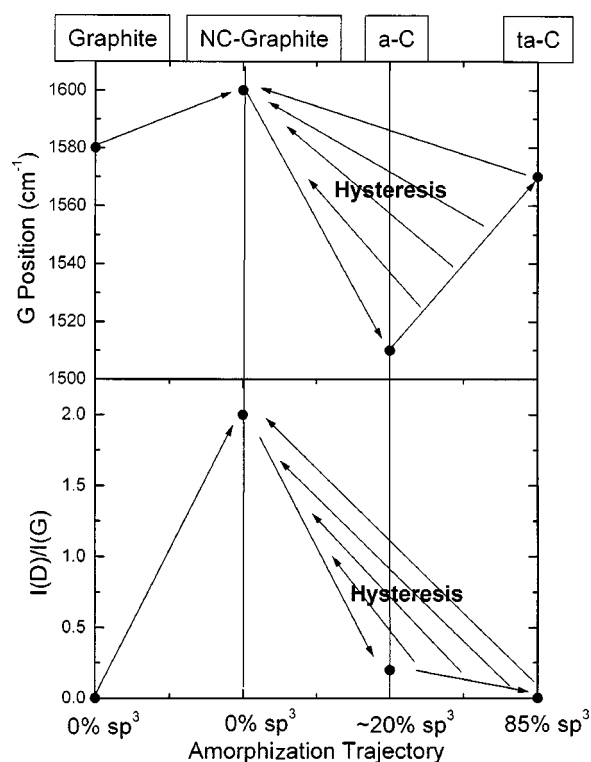


FIG. 10. Amorphization trajectory, showing the possibility of hysteresis in stages 2 and 3.

VIII. RELATIONSHIPS BETWEEN VISIBLE RAMAN SPECTRA AND THE sp^3 FRACTION IN a -C:H

More generally, if there is a relationship between sp^2 and sp^3 phases, e.g., between the optical gap and sp^3 fraction, we can derive sp^3 content from the visible Raman spectra. We apply this idea to derive a correlation between visible Raman spectra and sp^3 content for a -C:H.

The main effect of H in a -C:H is to modify its C-C network compared to a -C of similar sp^3 content. A higher sp^3 content is achieved mainly by H saturating C=C bonds as $\equiv\text{CH}_x$ groups, rather than by increasing the fraction of C—C bonds (Fig. 1). Most sp^3 sites are bonded to hydrogen.^{63,64} Thus, highly sp^3 a -C:H are soft, low-density, polymeric films.^{63,64} In a -C:H the sp^2 sites can exist as rings as well as chains. Increasing H content reduces the sp^2 cluster size and increases the band gap. We have three bonding regimes.^{1,63} At low H content, sp^2 bonding dominates and the gap is under 1 eV. At intermediate H content, the C—C sp^3 bonding is a maximum, the films have the highest density and diamondlike character, and the gap is 1–1.8 eV. At highest H contents, the sp^3 content is highest, the bonding is more polymeric, and the band gap is over 1.8 eV. ta -C:H differs in that a higher sp^3 fraction occurs at a fixed, lower H content of 25–30% (Fig. 1). ta -C:H has much more C—C sp^3 bonding than a -C:H with similar sp^3 fraction, giving a higher density and higher hardness.⁶⁵

In visible Raman spectra, we can neglect all C-H modes. The stretching modes lie above 3000 cm^{-1} .⁶⁴ C-H bending modes lie in the D -peak region,^{33,64} but we neglect them because they are not resonantly enhanced. This is supported by a similar behavior for D and G peaks with changing excitation energy found in a -C:H and a -C.^{10,11} C-H modes

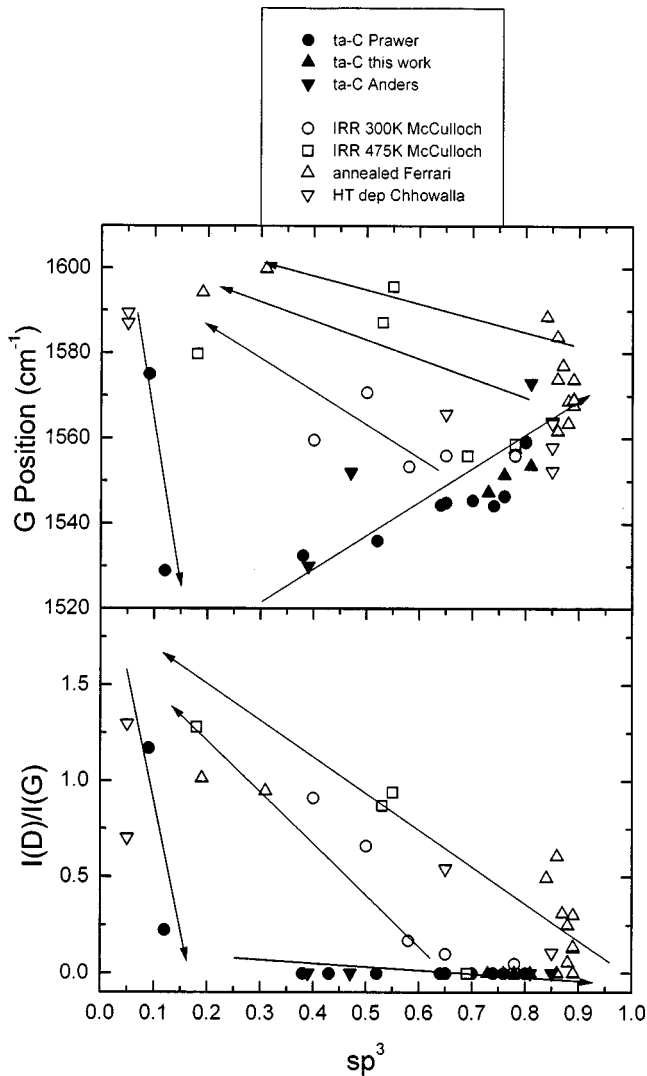


FIG. 11. G position and $I(D)/I(G)$ ratio data showing the hysteresis effect. Data on as deposited ta -C, from Prawer *et al.* (Ref. 42), this work, and Anders and co-workers (Refs. 56 and 59). Data on irradiated ta -C from McCulloch *et al.* (Refs. 61 and 62); on ta -C annealed after deposition from Ferrari *et al.* (Ref. 57); and on ta -C deposited at high temperature from Chhowalla *et al.* (Ref. 48).

could become detectable at much higher photon energy, such as that in uv Raman spectroscopy. A typical signature of hydrogenated samples is the increasing photoluminescence background with increasing H content. This background overshadows the Raman signal of a -C:H with H content over ~ 40 – 45 at. %⁶⁶ The ratio between the slope m of the fitted linear background and the intensity of the G peak, $m/I(G)$, could be used as a measure of the bonded H content.⁶⁶

We derive and explain the relation between visible Raman parameters and sp^3 content for a -C:H deposited by plasma-enhanced chemical vapor deposition (PECVD). From Tamor and Vassel¹³ we obtain a general relation between 514-nm Raman parameters and the optical gap for as-deposited a -C:H (Fig. 12). $I(D)/I(G)$ is now an area ratio of a two-Gaussian fit [thus giving $I(D)/I(G)$ up to ~ 4 , in contrast to ~ 2 obtained with the intensity ratio in a BWF+Lorentzian fit]. Figure 12(a) shows that the G peak falls with increasing gap for a -C:H, differently from ta -C, although the gap increases with sp^3 content in both materials. The reasons for

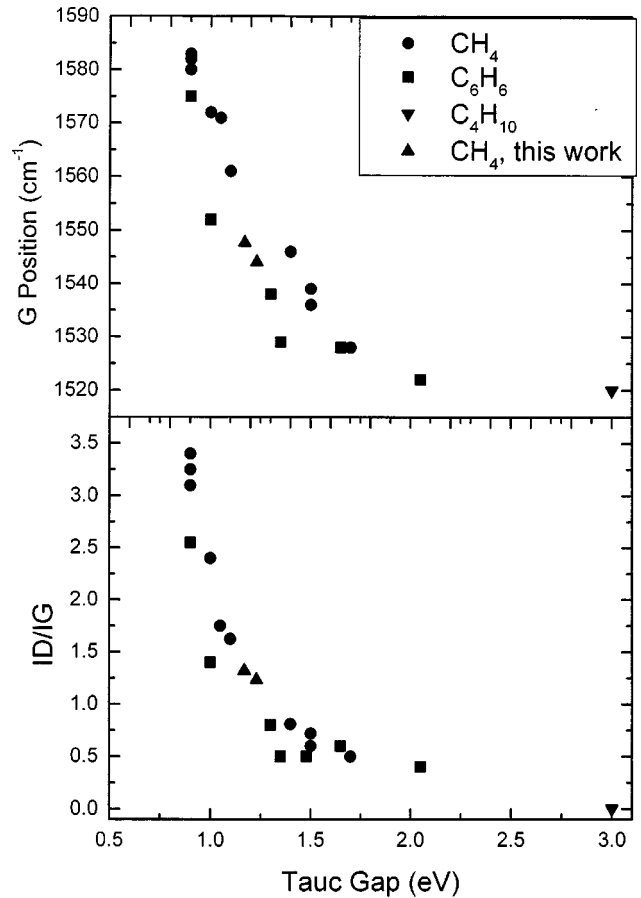


FIG. 12. G position and $I(D)/I(G)$ ratio vs optical Tauc gap for as-deposited a -C:H. Data from Tamor and Vassel (Ref. 13) and this work. The precursor gases are also indicated. Note that a double-Gaussian fit was used (Ref. 13).

the difference is that in a -C:H the C=C stretching frequencies tend to fall towards the lower values of under 1500 cm^{-1} seen in polyacetylene,^{33,55} whereas in ta -C the C=C stretching frequency tends to rise towards that of the embedded C=C dimer at 1630 cm^{-1} . The mixing with sp^3 modes also helps to lower the G peak in a -C:H.

For as-deposited a -C:H, there is a general relationship between sp^2 content and optical gap;⁶⁷ see Fig. 13. The line in Fig. 13 is a fit to the experimental data. Applying the fitting line to the data of Fig. 12, we obtain the relationship between sp^3 content and Raman parameters shown in Fig. 14. The crosses in Fig. 14 are for samples whose sp^3 content was directly measured (Ref. 68) by NMR or EELS (this work). They agree with the sp^3 content derived by Raman spectroscopy. Thus Raman spectroscopy is a valuable method to obtain sp^3 content for as-deposited a -C:H. Figures 12–14 will be improved by a further systematic study.

Figure 14 also shows Raman and sp^3 data for ta -C:H films deposited by an electron cyclotron wave resonance source from C_2H_2 .⁶⁵ The G peak of ta -C:H is seen to lie above that of a -C:H of similar sp^3 content (gap). These data show how the transition between the second and third stage also occurs in a -C:H, indicating how the three-stage model applies to both unhydrogenated and hydrogenated carbons.

It is important to note that the G peak in a -C:H and (t) a -C shows dispersion with photon energy, in both cases

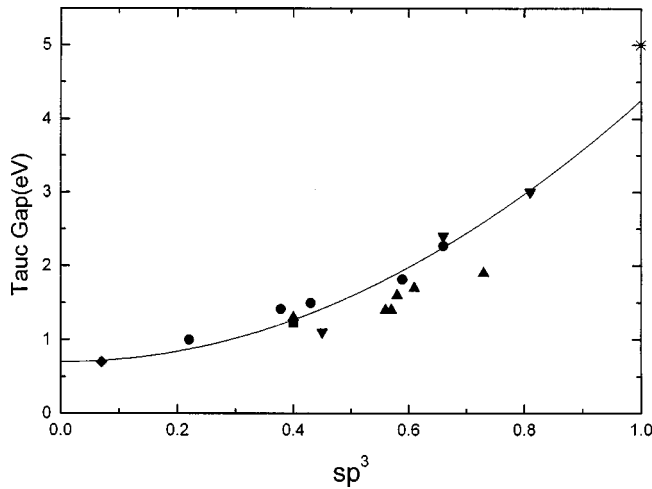


FIG. 13. Optical Tauc gap vs sp^3 content for as-deposited a -C:H. Data from Tamor and co-workers (●) (Refs. 13 and 68), Kleber *et al.* (▲) (Ref. 69), Jarman *et al.* (▼) (Ref. 70), Li and Lannin (◆) (Refs. 31 and 47), and this work (■). An ideal point at 5 eV is set to correspond to 100% sp^3 (*). The line is a quadratic fit to the data.

increasing for higher photon energies.^{10–12,15,16} Thus, the relations between the G position and gap or sp^3 fraction of Figs. 9, 12, and 14 apply for 514-nm excitation. The increased G position with increased excitation arises from the resonant selection of wider-band gap π states from sp^2 groups with higher vibration frequency. This leads to a lower sensitivity of the G position and $I(D)/I(G)$ to optical gaps with higher excitation energy,¹² since the optical gap is due to the more delocalized π -bonded structures.¹⁷ This would suggest that red Raman spectroscopy is preferable to the traditional green or blue spectroscopy to better exploit the ability of visible Raman spectra to follow the fine variations of optical gap on sp^2 order.

The width of the G peak is proportional to the bond-angle disorder at sp^2 sites. Figure 15 plots the G width (ΔG) against the optical gap for as-deposited a -C:H.¹³ It is seen that ΔG passes through a maximum at around 1.5 eV for a -C:H, which corresponds to films of maximum C-C sp^3 or “diamondlike” content.

As the skeletal structure of a -C:H depends strongly on its H content, we expect a strict relation between the H content and C-C structure during annealing of a -C:H. We therefore expect only a small hysteresis of the Raman parameters during annealing of a -C:H compared to the case of ta -C. Thus, relations in Figs. 12 and 14 are valid for both as-deposited and annealed a -C:H films. However, we expect hysteresis for ta -C:H.

IX. CONCLUSIONS

We have reviewed and critically assessed the origin and the meaning of the D and G peaks in the Raman spectra of graphite and amorphous carbons. We pointed out that the G peak is due to the relative motion of sp^2 carbon atoms, while the D peak is linked to breathing modes of rings. We showed how the electronic and vibration states of sp^2 aromatic clusters can be mapped onto those of graphite. The Raman spectra depend formally on the ordering of the sp^2 sites, due to

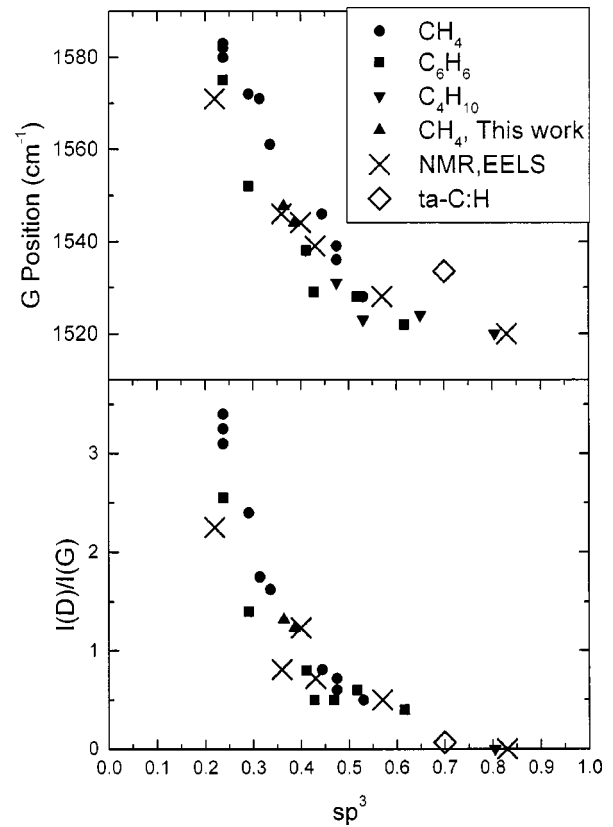


FIG. 14. G position and $I(D)/I(G)$ ratio vs sp^3 fraction for as-deposited a -C:H. The data are obtained applying the fit of Fig. 13 to data in Fig. 12. The \times symbols indicate samples for which sp^3 was directly measured by NMR (Ref. 68) or EELS (this work). The ta -C:H data point (\diamond) is shown for comparison; its sp^3 content was directly measured.

the resonant enhancement of their vibrations. We are able to classify all the available visible Raman data by considering the effect of a three-stage introduction of disorder into graphite on its Raman spectrum. We showed how this description applies both to hydrogen-free and hydrogenated amorphous carbons.

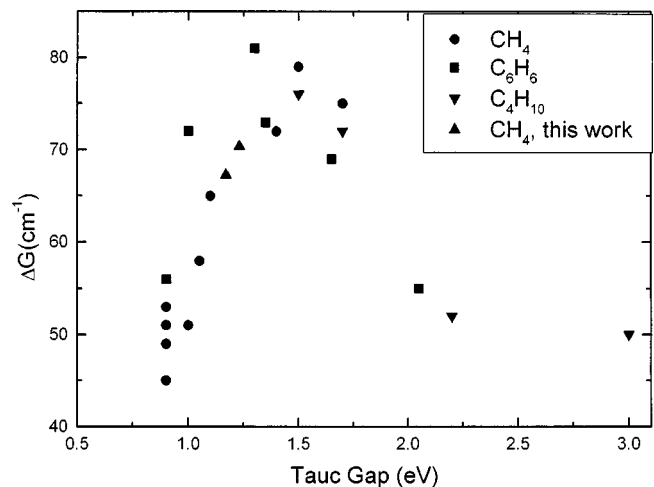


FIG. 15. ΔG vs the optical Tauc gap for as deposited a -C:H. Data from Tamor and Vassel (Ref. 13) and this work. Note that ΔG is the width of the Gaussian, not its FWHM (Ref. 13). The precursor gases are also indicated.

The ability to deduce sp^3 content from the visible Raman spectra depends on the linkage of sp^2 and sp^3 phases. In H-free (t) a -C, the clustering of sp^2 only depends on sp^3 content as-deposited, but generally not in films annealed, deposited at higher temperatures, or ion implanted. Thus, the sp^3 content can be deduced from their Raman spectra only for as-deposited ta -C. The C-C network of a -C:H depends strongly on its hydrogen content, which links the sp^2 and sp^3 phases together. This allows the sp^3 content of a -C:H to

be derived from the 514-nm Raman spectra. A relationship was given between the G -peak position, $I(D)/I(G)$, and sp^3 content.

ACKNOWLEDGMENTS

The authors are grateful to C. Mapelli and C. Castiglioni for useful discussions. A. C. F. would like to thank the European Union Marie Curie TMR for financial support.

*Electronic address: acf26@eng.cam.ac.uk

- ¹J. Robertson, Prog. Solid State Chem. **21**, 199 (1991); Pure Appl. Chem. **66**, 1789 (1994).
- ²D. S. Knight and W. B. White, J. Mater. Res. **4**, 385 (1989).
- ³F. Tuinstra and J. L. Koenig, J. Chem. Phys. **53**, 1126 (1970).
- ⁴R. J. Nemanich and S. A. Solin, Phys. Rev. B **20**, 392 (1979).
- ⁵P. Lespade, R. Al-Jishi, and M. S. Dresselhaus, Carbon **20**, 427 (1982).
- ⁶P. Lespade, A. Marchard, M. Couzi, and F. Cruege, Carbon **22**, 375 (1984).
- ⁷N. Wada, P. J. Gaczi, and A. Solin, J. Non-Cryst. Solids **35&36**, 543 (1980).
- ⁸S. R. Salis, D. J. Gardiner, M. Bowden, J. Savage, and D. Rodway, Diamond Relat. Mater. **5**, 589 (1996).
- ⁹R. O. Dillon, J. A. Woollam, and V. Katkanant, Phys. Rev. B **29**, 3482 (1984).
- ¹⁰M. Yoshikawa, N. Nagai, M. Matsuki, H. Fukuda, G. Katagiri, H. Ishida, A. Ishitani, and I. Nagai, Phys. Rev. B **46**, 7169 (1992).
- ¹¹J. Wagner, M. Ramsteiner, C. Wild, and P. Koidl, Phys. Rev. B **40**, 1817 (1989).
- ¹²M. A. Tamor, J. A. Haire, C. H. Wu, and K. C. Hass, Appl. Phys. Lett. **54**, 123 (1989).
- ¹³M. A. Tamor and W. C. Vassel, J. Appl. Phys. **76**, 3823 (1994).
- ¹⁴J. Schwan, S. Ulrich, V. Bathori, H. Erhardt, and S. R. P. Silva, J. Appl. Phys. **80**, 440 (1996).
- ¹⁵K. W. R. Gilkes, H. S. Sands, D. N. Batchelder, J. Robertson, and W. I. Milne, Appl. Phys. Lett. **70**, 1980 (1997).
- ¹⁶V. I. Merkulov, J. S. Lannin, C. H. Munro, S. A. Asher, V. S. Veerasamy, and W. I. Milne, Phys. Rev. Lett. **78**, 4869 (1997).
- ¹⁷J. Robertson and E. P. O'Reilly, Phys. Rev. B **35**, 2946 (1987); J. Robertson, Adv. Phys. **35**, 317 (1986).
- ¹⁸W. A. Harrison, Phys. Rev. B **8**, 4487 (1973).
- ¹⁹C. A. Coulson and H. C. Longuet-Higgins, Proc. R. Soc. London, Ser. A **191**, 39 (1947); **193**, 447 (1948).
- ²⁰J. Robertson, Diamond Relat. Mater. **4**, 297 (1995).
- ²¹C. Mapelli, C. Castiglioni, G. Zerbi, and K. Mullen, Phys. Rev. B **60**, 12 710 (1999); C. Mapelli, Tesi di Laurea, Politecnico di Milano, 1998.
- ²²G. Kresse, J. Furthmuller, and J. Hafner, Europhys. Lett. **32**, 729 (1995).
- ²³P. Pavone, K. Karch, O. Shutt, W. Windl, D. Strauch, P. Gianozzi, and S. Baroni, Phys. Rev. B **48**, 3164 (1993).
- ²⁴T. Kohler, T. Frauenheim, and G. Jungnickel, Phys. Rev. B **52**, 11 837 (1995).
- ²⁵A. Richter, H. J. Scheibe, W. Pompe, K. W. Brzezinka, and I. Muhling, J. Non-Cryst. Solids **88**, 131 (1986).
- ²⁶R. Alben, D. Weaire, J. E. Smith, and M. H. Brodsky, Phys. Rev. B **11**, 2271 (1975); D. Beeman and R. Alben, Adv. Phys. **26**, 339 (1977).
- ²⁷R. Al-Jishi and G. Dresselhaus, Phys. Rev. B **26**, 4514 (1982).
- ²⁸R. A. Jishi, L. Venkantaraman, M. S. Dresselhaus, and G. Dresselhaus, Chem. Phys. Lett. **209**, 77 (1993).
- ²⁹R. J. Nemanich, S. A. Solin, and R. M. Martin, Phys. Rev. B **23**, 6348 (1981).
- ³⁰R. Shuker and R. W. Gammon, Phys. Rev. Lett. **25**, 222 (1970).
- ³¹F. Li and J. S. Lannin, Appl. Phys. Lett. **61**, 2116 (1992).
- ³²G. P. Lopinski, V. I. Merkulov, and J. S. Lannin, Appl. Phys. Lett. **69**, 3348 (1996).
- ³³D. Lin-Vien, N. B. Colthup, W. G. Fateley, and J. G. Grasselli, *The Handbook of Infrared and Raman Characteristic Frequencies of Organic Molecules* (Academic, New York, 1991).
- ³⁴R. P. Vidano, D. B. Fishbach, L. J. Willis, and T. M. Loehr, Solid State Commun. **39**, 341 (1981).
- ³⁵A. V. Baranov, A. N. Bekhterev, Y. S. Bobovich, and V. I. Petrov, Opt. Spektrosk. **62**, 1036 (1987) [Opt. Spectrosc. **62**, 612 (1987)].
- ³⁶I. Pocsik, M. Hundhausen, M. Koos, and L. Ley, J. Non-Cryst. Solids **227-230**, 1083 (1998).
- ³⁷M. J. Matthews, M. A. Pimenta, G. Dresselhaus, M. S. Dresselhaus, and M. Endo, Phys. Rev. B **59**, 6585 (1999).
- ³⁸P. Y. Yu and M. Cardona, *Fundamentals of Semiconductors* (Springer-Verlag, Berlin, 1996).
- ³⁹P. Tan, Y. Deng, and Q. Zhao, Phys. Rev. B **58**, 5435 (1998).
- ⁴⁰D. G. McCulloch, S. Prawer, and A. Hoffman, Phys. Rev. B **50**, 5905 (1994).
- ⁴¹D. G. McCulloch and S. Prawer, J. Appl. Phys. **78**, 3040 (1995).
- ⁴²S. Prawer, K. W. Nugent, Y. Lifshitz, G. D. Lempert, E. Grossman, J. Kulik, I. Avigal, and R. Kalish, Diamond Relat. Mater. **5**, 433 (1996).
- ⁴³M. V. Klein, in *Light Scattering in Solids III*, edited by M. Cardona and G. Guntherodt, Topics in Applied Physics Vol. 51 (Springer-Verlag, Berlin, 1982).
- ⁴⁴D. Beeman, J. Silverman, R. Lynds, and M. R. Anderson, Phys. Rev. B **30**, 870 (1984).
- ⁴⁵S. Prawer, K. W. Nugent, D. N. Jamieson, Diamond Relat. Mater. **7**, 106 (1998); J. D. Hund, S. P. Withrow, C. W. White, and D. M. Hembree, Phys. Rev. B **52**, 8106 (1995).
- ⁴⁶A. Cuesta, P. Dhamelin-court, J. Laureyns, A. Martinez-Alonso, and J. M. D. Tascon, J. Mater. Chem. **8**, 2875 (1998); H. Wilhelm, M. Lelaurain, E. McRae, and B. Humbert, J. Appl. Phys. **84**, 6552 (1998).
- ⁴⁷F. Li and J. S. Lannin, Phys. Rev. Lett. **65**, 1905 (1990).
- ⁴⁸M. Chhowalla, A. C. Ferrari, J. Robertson, and G. A. J. Amaratunga, Appl. Phys. Lett. **76**, 1419 (2000).
- ⁴⁹F. Parmigiani, E. Klay, and H. Seki, J. Appl. Phys. **64**, 3031 (1988).
- ⁵⁰G. Galli, R. A. Martin, R. Car, and M. Parrinello, Phys. Rev. Lett. **62**, 555 (1989).
- ⁵¹U. Stephan, T. Frauenheim, P. Blaudeck, and J. Jungnickel, Phys. Rev. B **49**, 1489 (1994).

- ⁵²K. W. R. Gilkes, P. H. Gaskell, and J. Robertson, *Phys. Rev. B* **51**, 12 303 (1995).
- ⁵³D. A. Drabold, P. A. Fedders, and P. Strumm, *Phys. Rev. B* **49**, 16 415 (1994).
- ⁵⁴N. A. Marks, D. R. McKenzie, B. A. Pailthorpe, M. Bernasconi, and M. Parrinello, *Phys. Rev. B* **54**, 9703 (1996).
- ⁵⁵Y. Yacoby and E. Ehrenfreund, in *Light Scattering in Solid IV*, edited by M. Cardona and G. Guntherodt (Springer-Verlag, Berlin, 1991).
- ⁵⁶J. W. Ager, S. Anders, A. Anders, and I. G. Brown, *Appl. Phys. Lett.* **66**, 3444 (1995).
- ⁵⁷A. C. Ferrari, B. Kleinsorge, N. A. Morrison, A. Hart, V. Stolojan, and J. Robertson, *J. Appl. Phys.* **85**, 7191 (1999).
- ⁵⁸T. A. Friedmann, J. P. Sullivan, J. A. Knapp, D. R. Tallant, D. M. Follstaedt, D. L. Medlin, and P. B. Mirkarimi, *Appl. Phys. Lett.* **71**, 3820 (1997).
- ⁵⁹S. Anders, J. W. Ager, G. M. Pharr, T. Y. Tsui, and I. G. Brown, *Thin Solid Films* **308**, 186 (1997).
- ⁶⁰D. R. Tallant, T. A. Friedmann, N. A. Missert, M. P. Siegal, and J. P. Sullivan, in *Covalently Bonded Disordered Thin-Film Materials*, edited by M. P. Siegal *et al.*, MRS Symposia Proceedings No. 498 (Materials Research Society, Pittsburgh, 1998), p. 37.
- ⁶¹D. G. McCulloch, E. G. Gerstner, D. R. McKenzie, S. Prawer, and R. Kalish, *Phys. Rev. B* **52**, 850 (1995).
- ⁶²D. G. McCulloch, D. R. McKenzie, S. Prawer, A. R. Merchant, E. G. Gerstner, and R. Kalish, *Diamond Relat. Mater.* **6**, 1622 (1997).
- ⁶³P. Koidl, C. Wagner, B. Dischler, J. Wagner, and M. Ramsteiner, *Mater. Sci. Forum* **52**, 41 (1990).
- ⁶⁴J. Ristein, R. T. Stief, L. Ley, and W. Beyer, *J. Appl. Phys.* **84**, 3836 (1998).
- ⁶⁵N. A. Morrison, S. E. Rodil, A. C. Ferrari, J. Robertson, and W. I. Milne, *Thin Solid Films* **337**, 71 (1999).
- ⁶⁶B. Marchon, J. Gui, K. Grannen, G. C. Rauch, J. W. Ager, S. R. P. Silva, and J. Robertson, *IEEE Trans. Magn.* **33**, 3148 (1997).
- ⁶⁷J. Robertson, *Philos. Mag. B* **76**, 335 (1997).
- ⁶⁸M. A. Tamor, W. C. Vassel, and K. R. Carduner, *Appl. Phys. Lett.* **58**, 592 (1991).
- ⁶⁹R. Kleber, K. Jung, H. Ehrhardt, I. Muhling, K. Breuer, H. Metz, and F. Engelke, *Thin Solid Films* **205**, 274 (1991).
- ⁷⁰R. H. Jarman, G. J. Ray, R. W. Stanley, and G. W. Zajac, *Appl. Phys. Lett.* **49**, 1065 (1986).